European Polymer Journal 116 (2019) 1–8

Contents lists available at ScienceDirect

European Polymer Journal

journal homepage: www.elsevier.com/locate/europolj

Synthesis, mechanical properties and biodegradation of various acrylic acid-grafted poly(butylene succinate-co-terephthalate)/organically modified layered zinc phenylphosphonate nanocomposites

Sheng-Hsiang Lin, Jie-Mao Wang, Hsiang-Ting Wang, Tzong-Ming Wu*

Department of Materials Science and Engineering, National Chung Hsing University, 250 Kuo Kuang Road, Taichung 402, Taiwan

ARTICLE INFO

Keywords:
Biodegradable
Aliphatic-aromatic copolyesters
Composites
Mechanical property
Thermal stability

ABSTRACT

A new series of biodegradable aliphatic-aromatic nanocomposites containing various acrylic acid-grafted poly (butylene succinate-co-terephthalate) (PBST) and organically modified layered zinc phenylphosphonate (m-PPZn) were successfully synthesized through the transesterification and polycondensation having the covalent linkages between polymer and inorganic materials. Fourier transform infrared (FTIR) and ^{13}C-nuclear magnetic resonance (NMR) spectra demonstrate the successful grafting of acrylic acid to PBST (g-PBST). Both wide-angle X-ray diffraction and transmission electron microscopy data show that the g-PBST polymer matrix was intercalated into the interlayer spacing of m-PPZn. The additional m-PPZn into g-PBST matrix significantly enhanced the storage modulus as compared with that of neat g-PBST. The reduction in thermal stability was observed in all g-PBST/m-PPZn systems, which is probably caused by more nucleation to form more tiny and imperfect crystals. The biodegradations of neat g-PBST copolymers and g-PBST/m-PPZn nanocomposites were investigated using lipase from *Pseudomonas* sp. The degradation rates of the neat g-PBST copolymers increased in the order of g-PBST-70 > g-PBST-50 > g-PBST-30. The faster degradation rate of g-PBST-70 is a result of a higher content of succinic acid unit and chain flexibility of polymer backbone. Furthermore, the weight loss increased by increasing the loading of m-PPZn, suggesting that the existence of m-PPZn improved the degradation of the g-PBST copolymers.

1. Introduction

Aliphatic-aromatic copolyesters have attracted great interest owing to their promising biodegradability of aliphatic units and excellent mechanical properties of aromatic units in their polymer backbones [1,2]. Poly(butylene succinate-co-terephthalate) (PBST), one of the important aliphatic-aromatic copolymers, is synthesized via transesterification and polycondensation of 1,4-butanediol (BD) in the presence of succinic acid (SA) and terephthalic acid (TPA) or dimethylene terephthalate (DMT) [3–6]. Because of the presence of aromatic unit of TPA or DMT, PBST has been intensively investigated owing to its outstanding mechanical and thermal properties as compared with another biodegradable poly(butylene succinate-*co*-adipate) [7–9]. PBST can also reduce oil consumption since raw materials of BD and SA are obtained from bio-ferment. However, the relatively slow crystallization rate and unstable morphologies in the manufacturing process could limit its extensive applications and development. The loading of stiff inorganic materials acting as nucleating agents and reinforcement materials into the aliphatic-aromatic copolymers can further accelerate their crystallization rates and enhance their mechanical and thermal properties [10–12]. Wei et al. investigated the influence of silica nanoparticles on the crystallization as well as on the mechanical and thermal properties of PBST/silica nanocomposites [10]. As a result, the incorporation of silica nanoparticles improved the mechanical and thermal properties of PBST. The major contribution of silica nanoparticles was to accelerate the crystallization rate of PBST. Wei et al. also reported that the incorporation of fibrous attapulgite nanoparticles can accelerate the crystallization rate as well as improve the mechanical properties of PBST. The above investigations reveal that polymer and inorganic material share a non-covalent interaction. Normally, covalent linkages between the polymer and inorganic materials using “grafting to” or grafting from” approach have been employed to bind polymer chains onto the surface [13,14]. These approaches are more stable and could significantly enhance the physical properties compared to those fabricated using non-covalent bond.

Two-dimensional layered zinc phenylphosphonate (PPZn) has

* Corresponding author at: 250 Kuo Kuang Road, Taichung 402, Taiwan.
E-mail address: tmwu@dragon.nchu.edu.tw (T.-M. Wu).

https://doi.org/10.1016/j.eurpolymj.2019.03.061
Received 29 October 2018; Received in revised form 24 March 2019; Accepted 30 March 2019
Available online 02 April 2019
0014-3057/

attracted immense attention owing to its ability to accelerate crystallization rates of numerous polymers [15–17]. To create the covalent linkages between PPZn and PBST, organo-modifiers having at least two functional groups and chemical modification of PBST are necessary. In this study, biocompatible and nontoxic 1, 12-dodecanediamine was applied to manufacture the organically-modified PPZn (m-PPZn) via a co-precipitation method.

In this study, a series of new biodegradable composites containing various acrylic acid-grafted poly(butylene succinate-co-terephthalate) (g-PBST) and organically modified layered PPZn were successfully synthesized with covalent linkages between the polymer and inorganic materials. To the best of our knowledge, the g-PBST/m-PPZn nanocomposites with covalent linkages between g-PBST and m-PPZn are reported for the first time. The mechanical, thermal and biodegradable properties of g-PBST/m-PPZn nanocomposites were systematically studied.

2. Material and methods

2.1. Materials

Phenylphosphonic acid, succinic acid (SA), titanium(IV) isopropoxide, zinc nitrate and lipase from *Pseudomonas* sp. were acquired from Sigma-Aldrich Chemical Company. Acrylic acid (AA), azobisisobutyronitrile (AIBN), 1,4-butanediol (BD), dimethylene terephthalate (DMT), 1,12-dodecanediamine, 1-ethyl-3-(3-dimethylaminopropyl)carbodiimide (EDC), and tetrabutyl titanate were obtained from Alfa Aesar Chemical Company. All chemicals were used without purification.

2.2. Fabrication of g-PBST/m-PPZn nanocomposites

Three different molar ratios of PBST were synthesized via transesterification and polycondensation, which has been reported previously [3–5]. The feed molar ratios of [SA] to [DMT] were 30:70, 50:50, and 70:30 and designated amounts of BD; the resulting products are hereinafter designated as PBST-30, PBST-50, and PBST-70, respectively. In brief, desirable amounts of SA, DMT, BD and titanium(IV) isopropoxide as a catalyst were heated and mechanically stirred at 165 °C for 30 mins in a stream of nitrogen gas, and then heated to 200 °C for 2 hrs in a vacuum of 0.4 ~ 0.5 torr, and finally 240 °C for 3 h. The as-prepared PBST was dissolved in chloroform, and then precipitated from cold methanol for purification.

The modification of PBST and PPZn and the fabrication of the resulting composite materials are shown in Fig. 1. The obtained PBST was dissolved in chloroform and a mixture of AA and AIBN were added to the prepared solution at 60 °C for 24 h to permit grafting reaction to occur (hereafter designated as g-PBST). The PPZn and 1,12-dodecanediamine-modified PPZn (m-PPZn) were prepared according to the methods reported in previous studies [18,19]. Different amounts of g-PBST, m-PPZn and EDC as a catalyst were individually dissolved in dichloromethane, and then mixed/mechanically stirred for 3 days. The obtained g-PBST/m-PPZn nanocomposites were washed and dried in vacuum. The nanocomposite are identified as *x*wt% g-PBST/m-PPZn, where *x*wt% is the weight percent of m-PPZn.

2.3. Morphology of g-PBST/m-PPZn nanocomposites

X-ray diffractometer (Bruker D8) equipped with a Ni-filtered Cu Kα radiation was used for the experiments of wide-angle X-ray diffraction (WAXD). The measurements of WAXD were carried out in the range of 2θ = 1.5°–30° at 1°/min. The transmission electron microscopy (TEM) was performed using Hitachi HF-2000. The samples of TEM experiments encapsulated by epoxy were operated by a Reichert Ultracut ultramicrotome.

2.4. FTIR analysis of g-PBST/m-PPZn nanocomposites

Fourier transform infrared (FTIR) experiments were carried out on a Perkin-Elmer Spectrum One spectrometer from 400 to 4000 cm^{-1}.

2.5. Crystallization behavior of g-PBST/m-PPZn nanocomposites

The crystallization behavior was carried out by a PerkinElmer Pyris Diamond DSC and all experiments were performed under nitrogen environment. All specimens were heated to the designed temperatures (T_{ds}), which are about 50 °C higher than the melting temperatures of g-PBST, at a rate of 10 °C/min and held for 5 min to remove the residual crystals. Then, they were cooled to −50 °C at a rate of 10 °C/min. Finally the samples were heated to T_{ds} at a rate of 10 °C/min and the crystalline melting temperature (T_m) for the g-PBST and g-PBST/m-PPZn nanocomposites are obtained. The degree of crystallinity (Xc) was evaluated by the enthalpy of fusion (ΔH_f). The thermal behaviors of specimens were operated using Perkin Elmer TG/DTA 6300 thermoanalyzer. These measurements were obtained from room temperature to 800 °C under a nitrogen environment at a heating rate of 10 °C/min.

2.6. NMR, XPS and GPC analysis of g-PBST/m-PPZn nanocomposites

^{1}H-nuclear magnetic resonance (NMR) and ^{13}C NMR spectra was obtained with Agilet Technologies DD2 600 MHz NMR spectrometer using $CDCl_3$ as solvent and internal standard. X-ray photoelectron spectroscopy (XPS) analysis was carried out on a PHI 5000 Versa Probe X-ray photoelectron spectrometer with the incident radiation consisting of Mg Kα X-ray and the takeoff angle fixed at 45°. The gel permeation chromatography (GPC; Waters 717 Plusautosampler, Waters Instruments, Rochester, NY, USA) was used to determine the number-average molecular weight (M_n), weight-average molecular weight (M_w), and polydispersity PDI = M_n/M_w of the resulting polymers and composite materials. Polystyrene standards with narrow molecular-weight distributions were used as calibration.

2.7. DMA analysis of g-PBST/m-PPZn nanocomposites

The storage modulus (E') was operated on a Perkin Elmer dynamic mechanical analyzer (DMA) from −80 to 100 °C at 2 °C/min heating rate and 1 Hz constant frequency.

2.8. Enzymatic degradation of g-PBST/m-PPZn nanocomposites

All samples for enzymatic degradation test were put in 24-well plates including 1 ml/mg lipase from *Pseudomonas sp*. The samples were removed at 3, 6, 9, and 12 days, washed with distilled water and vacuum dried. The quantity of degradation was estimated by means of the equation: $W_{weight\ loss}$ (%) = 100[($W_0 - W_t$)/W_0], where W_0 is the original weight of a sample and W_t corresponds to the weight of a sample after various degradation periods. The experimental data obtained here are the average values of at least three experiments.

3. Results and discussion

3.1. Synthesis and structure of various g-PBST copolymers

Different compositions of PBST copolyesters were determined via ^{1}H NMR spectroscopy. Fig. 2 shows the ^{1}H NMR data of the PBST-30 copolymers. The signals at δ = 8.11 and 2.64 ppm correspond to the hydrogen proton of phenyl for the terephthalate unit and the hydrogen proton of methylene group for the succinate unit, respectively [3]. The signal at δ = 7.26 ppm is attributed to the chloroform solvent. Four signals in a range of 4.50–4.00 and 2.00–1.50 ppm are contributed to the proton resonance of butanediol unit. For example, the integrated resonance intensities for these peaks at δ = 4.43, 4.35, 4.19, and

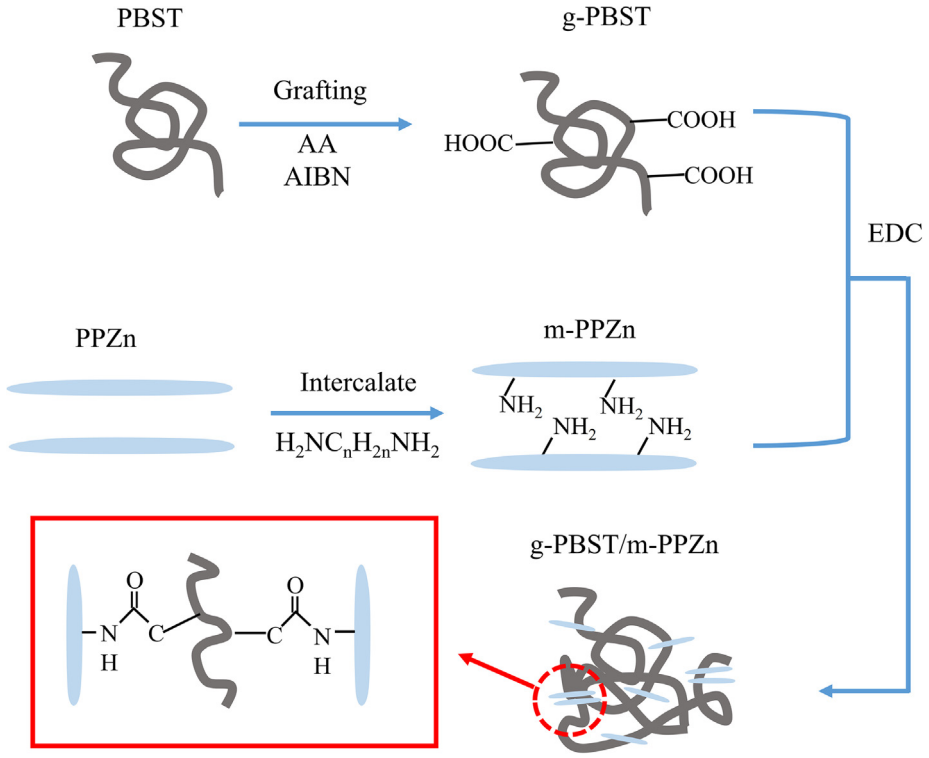

Fig. 1. Reaction scheme for the modification of PBST and m-PPZn and the fabrication of composite materials.

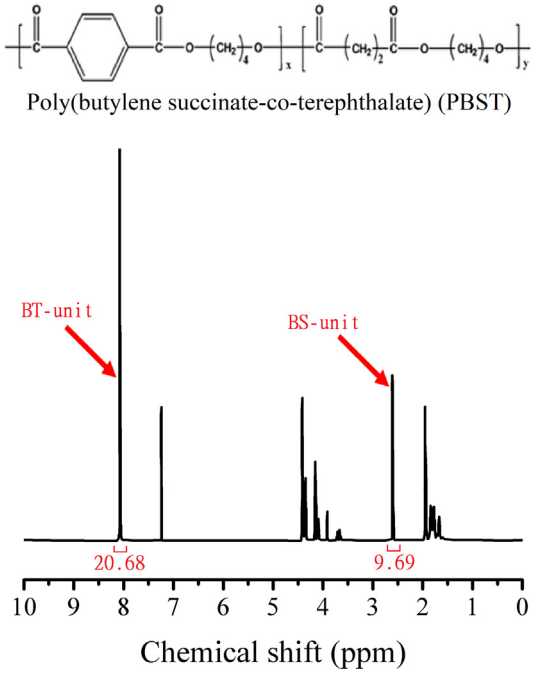

Fig. 2. ^{1}H NMR spectrum of the PBST-30 copolyester.

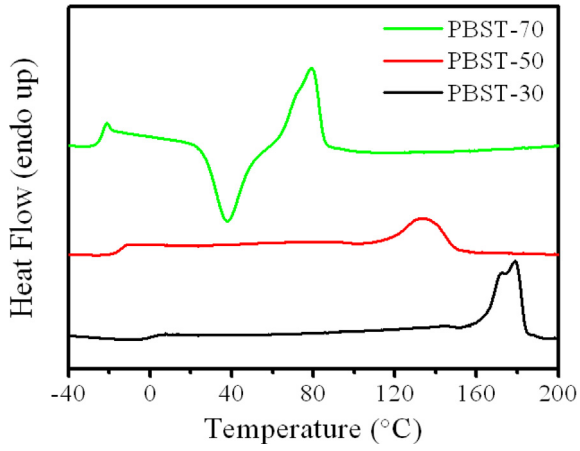

Fig. 3. DSC heating scans of the PBST copolymers.

4.11 ppm were accordingly assigned to the contributions from corresponding TBT, TBS, SBT, and SBS diad sequences, respectively [4,6]. Table 1 illustrates the chemical composition of PBST-30 copolyester calculated using the peak area ratio at δ = 2.64 ppm to 8.11 ppm. The ratio of succinate unit to terephthalate unit is almost equivalent to the feed ratio of [SA] to [DMT], suggesting that the composition of the synthesized PBST is in agreement with that calculated approximately on the basis of the feed ratio. Similar results for the fabricated PBST

Table 1
Composition and molecular weight of synthesized polyesters.

Polymer	Feed Ratio[SA]/[DMT] (mol %)	Polymer Ratio[a] [SA]/[DMT] (mol %)	M_w (g/mol) × 10^4	M_n (g/mol) × 10^4	PDI	Tg (°C)	T_m (°C)
PBST-30	30/70	31.9:68.1	5.18	2.92	1.77	−0.86	173.1
PBST-50	50/50	50.2:49.8	5.60	3.25	1.72	−15.7	130.1
PBST-70	70/30	70.5:29.5	5.98	3.56	1.68	−24.2	81.0

[a] Composition measured by ^{1}H NMR.

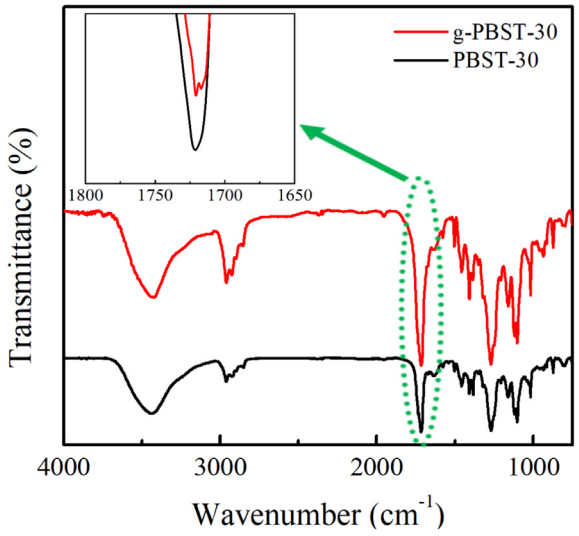

Fig. 4. FTIR spectra of the PBST-30 and g-PBST-30 copolyesters.

copolymers with different [SA]/[DMT] compositions are also recorded in Table 1. The molecular weights of the various PBST copolymers determined using GPC are also given in Table 1. The number average molecular weight (M_n) and polydisperse indices (PDI) of synthesized PBST copolymers were in the range of 29200 ~ 35600 g/mol and 1.68 ~ 1.77, respectively. Fig. 3 shows DSC heating scans of different compositions of PBST copolyesters. The melting temperatures of PBST determined by DSC are 173.1 °C, 130.1 °C, and 81.0 °C for PBST-30, PBST-50, and PSBT-70, respectively. The glass transition temperatures of various PBST copolymers are also given in Table 1.

Fig. 4 shows the FTIR spectra of PBST-30 and g-PBST-30. The characteristic absorption peaks of PBST-30 and g-PBST-30 around 1155 and 1243 cm^{-1} are attributed to the stretching of −COC− bonds in the ester group [20]. The peak at 1044 cm^{-1} corresponds to the stretching vibration of O-C-C bonds in the polymer. The absorption peak at 1721 cm^{-1} is assigned to the stretching vibration of the ester group, exclusively in the −C═O bonds of the carbonyl. An additional peak at 1717 cm^{-1} assigned to O−C═O was obtained in the modified PBST, which indicates the presence of free acid in the modified polymer. This result demonstrates the successful grafting of AA to PBST. Similar results are described in earlier literatures [13,21,22]. Further evidence for the grafting formation of AA shown in Fig. 5 is presented using the ^{13}C

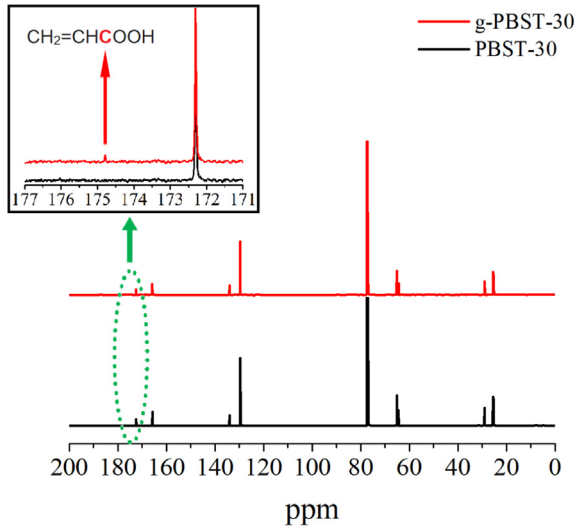

Fig. 5. ^{13}C NMR spectra of the PBST-30 and g-PBST-30 copolyesters.

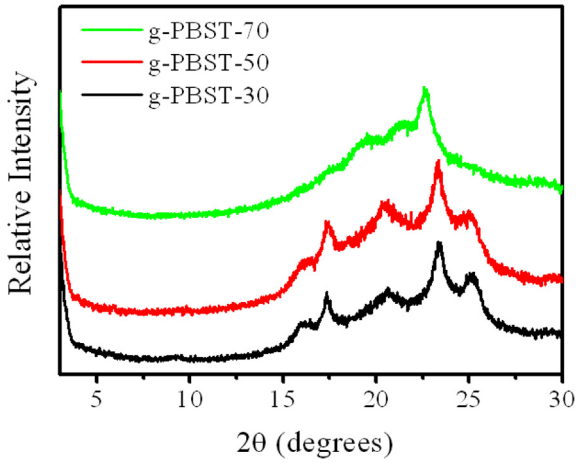

Fig. 6. WAXD patterns of g-PBST copolymers.

NMR spectra. Relative to that of neat PBST-30, the ^{13}C NMR spectra of g-PBST-30 contains an additional and small peak at δ = 174.8 ppm. This peak is contributed to the O−C═O bond of AA, which confirms the grafting of AA to PBST as well [19,20].

Fig. 6 reveals the WAXD diffraction curves of different compositions of g-PBST copolyesters. The diffraction peaks at 2θ = 16.2°, 17.3°, 20.6°, 23.4°, and 25.3° were observed for the g-PBST-30 and g-PBST-50 samples, which are consistent with those of crystalline PBT [6,23]. These findings demonstrate that the crystal structures of g-PBST-30 and g-PBST-50 were dominated by the crystalline PBT. As shown in this figure, the diffraction profiles of the g-PBST-70 copolymers at 2θ = 19.7°, 21.3°, and 22.7° are in good agreement with those of crystalline PBS [6]. This data reveals that the prepared g-PBST-70 copolymer was shifted from the crystalline structure of PBT into the crystalline structure of PBS. The melting temperatures of g-PBST determined by DSC were 178.9 °C, 133.3 °C, and 79.1 °C for g-PBST-30, g-PBST-50, and g-PSBT-70, respectively. The degree of crystallinity (Xc) evaluated by the enthalpy of fusion (ΔH_f) of DSC heating data is shown in Table 2.

3.2. Structure and morphology of various g-PBST/m-PPZn nanocomposites

Fig. 7 shows the FTIR spectra of g-PBST-30 and 5 wt% g-PBST-30/m-PPZn nanocomposites. The absorption peak at 1717 cm^{-1} assigned to −C═O of free acid is contributed to the presence of AA in the modified polymer. The FTIR spectrum of 5 wt% g-PBST-30/m-PPZn nanocomposites shows that the small shoulder peak at1717 cm^{-1} slightly shifted to 1714 cm^{-1} because of condensation and amide formation between carboxylic acid groups of g-PBST and amino groups of m-PPZn. This result demonstrates the successful formation of covalent linkages (amide groups) for 5 wt% g-PBST-30/m-PPZn nanocomposites. Similar results have been previously reported in the literatures [22,24]. Further evidence for the formation of amide linkages shown in Fig. 8 is presented using the ^{13}C NMR spectra. Relative to that of neat g-PBST-30, the peak at δ = 174.8 ppm contributed to the O−C═O bond of AA disappears in the ^{13}C NMR spectra of g-PBST-30/m-PPZn nanocomposites. At the same time, an additional and small peak at δ = 172.4 ppm is observed for the composite materials, which is attributed to the amide linkages of the materials [13]. In order to understand the formation of amide linkages for the g-PBST-30/m-PPZn nanocomposites, XPS analysis is a powerful tool to characterize the change of chemical composition for the g-PBST-30 and its composite. Fig. 9 show the XPS data of the g-PBST-30 copolyester and g-PBST/m-PPZn nanocomposite. It is clear that the intensity ratio of oxygen significantly decreases and additional peak of nitrogen at the binding energy (BE) of 400 eV for the g-PBST/m-PPZn nanocomposite. This results is consistent with the

Table 2
Initial degradation temperature, temperature of the maximum degradation rate, storage modulus at −70 °C and weight loss after 12 days degradation time of the various g-PBST/m-PPZn nanocomposites.

Sample	[a]T_d^i (°C)	[b]T_d^{max} (°C)	E' (MPa)	[c]Xc (%)	Weight loss (%)
g-PBST-30	379.6	406.4	1340	19.6	0
1 wt% g-PBST-30/m-PPZn	373.2	399.7	1450	18.9	0.93
3 wt% g-PBST-30/m-PPZn	373.7	399.5	1760	17.5	2.27
5 wt% g-PBST-30/m-PPZn	369.3	399.7	1950	17.3	4.42
g-PBST-50	375.7	403.4	1550	12.5	3.12
1 wt% g-PBST-50/m-PPZn	368.6	397.4	1740	11.4	7.05
3 wt% g-PBST-50/m-PPZn	365.0	394.5	2130	11.1	7.37
5 wt% g-PBST-50/m-PPZn	365.9	394.5	2250	11.0	9.70
g-PBST-70	374.3	404.0	2010	17.4	52.3
1 wt% g-PBST-70/m-PPZn	372.7	395.7	2120	16.6	61.5
3 wt% g-PBST-70/m-PPZn	369.7	394.8	2350	16.2	72.5
5 wt% g-PBST-70/m-PPZn	369.8	394.8	2790	16.0	86.7

$X_c(\%) = \frac{\Delta H_f}{(1-\phi)\Delta H_f^0} \times 100\%$.

[a] T_d^i: Initial degradation temperature.

[b] T_d^{max}: Temperature of the maximum degradation rate.

[c] Xc: Crystallinity is obtained by the following equation using $\Delta H_f{}^0$ = 144.5 J/g for PBST-30 and PBST-50, $\Delta H_f{}^0$ = 110.5 J/g for PBST-70, and φ is the weight fraction of the m-PPZn in the nanocomposites [6].

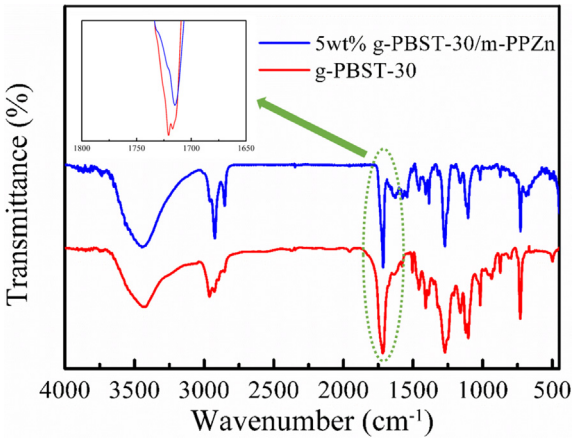

Fig. 7. FTIR spectra of the g-PBST-30 copolyester and g-PBST/m-PPZn nanocomposite.

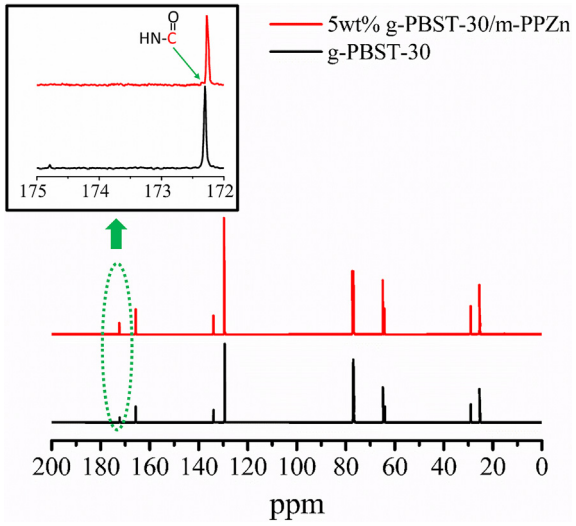

Fig. 8. ^{13}C NMR spectra of the g-PBST-30 copolyester and g-PBST/m-PPZn nanocomposite.

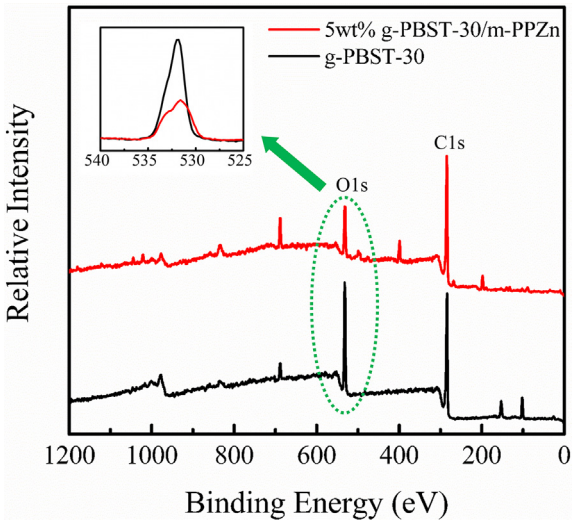

Fig. 9. XPS data of the g-PBST-30 copolyester and g-PBST/m-PPZn nanocomposite.

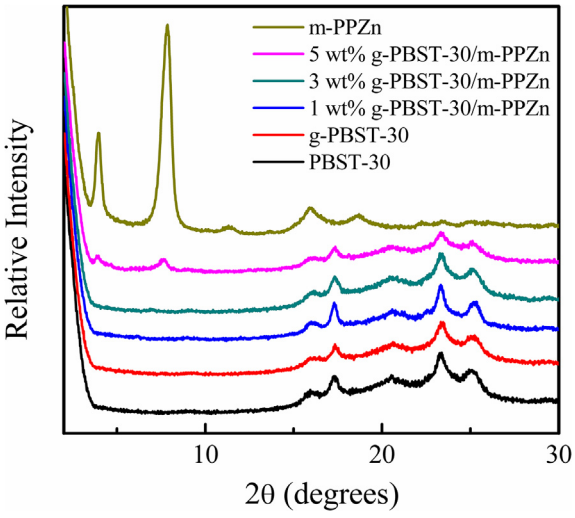

Fig. 10. WAXD patterns of PBST-30, g-PBST-30, m-PPZn and various weight ratio of g-PBST-30/m-PPZn nanocomposites.

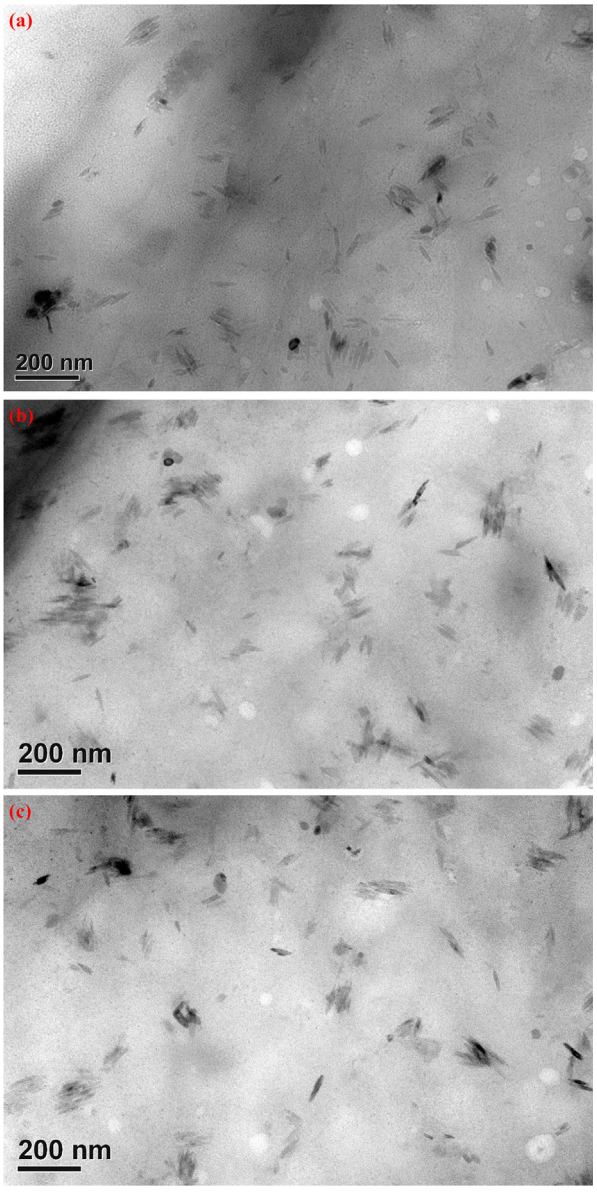

Fig. 11. TEM micrographs of 5 wt% (a) g-PBST-30/m-PPZn, (b) g-PBST-50/m-PPZn and (c) g-PBST-70/m-PPZn nanocomposites.

structure change from the O—C═O formation of g-PBST-30 to N—C═O formation of g-PBST-30/m-PPZn nanocomposites.

WAXD diffraction profiles of the g-PBST-30/m-PPZn nanocomposites are presented in Fig. 10. For comparison, the X-ray diffraction data of m-PPZn is also shown in this figure. A small trace of diffraction peak at $2\theta = 5.5^{\circ}$ was clearly obtained in the experimental results of higher m-PPZn loading specimens, which contributes to the presence of the stacking layers of m-PPZn. These results suggest that the intercalated conformation was formed for the g-PBST-30/m-PPZn nanocomposites. Similar results were also obtained for the g-PBST-50/m-PPZn and g-PBST-70/m-PPZn nanocomposites. Furthermore, the morphologies of 5 wt% g-PBST/m-PPZn nanocomposites were directly examined using TEM. Fig. 11 illustrates the TEM images of 5 wt% loading of m-PPZn into g-PBST-30, g-PBST-50, and g-PBST-70 copolymer matrices. These images indicate that the stacking layers of m-PPZn were intercalated within the g-PBST copolyesters. Consequently, the intercalated morphologies of g-PBST/m-PPZn nanocomposites imaged via TEM here are in good agreement with the diffraction data of WAXD.

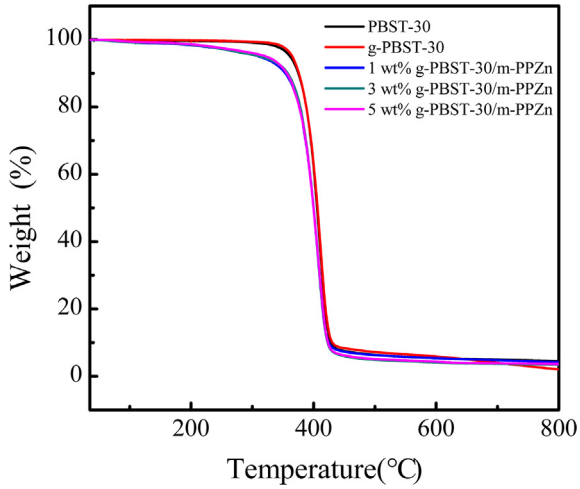

Fig. 12. TGA profiles of PBST-30, g-PBST-30 and various weight ratio of g-PBST-30/m-PPZn nanocomposites.

3.3. Physical properties of various g-PBST/m-PPZn nanocomposites

TGA analysis was used to study the effect of m-PPZn on the thermal degradation of various g-PBST matrices. Fig. 12 shows the TGA profiles of the g-PBST-30/m-PPZn nanocomposites. The experimental data for the g-PBST-50/m-PPZn and g-PBST-70/m-PPZn nanocomposites present a similar trend. The degradation temperatures gained from these patterns are summarized in Table 2. As presented in this table, the initial mass loss temperature of neat g-PBST-30 is higher than those of g-PBST-50 and g-PBST-70. These experimental observations disclose that neat g-PBST-30 displayed the best thermal stability among these synthesized copolyesters, analogous to previously reported results of PBST copolymers without grafting reaction [4,11]. Nevertheless, the degradation temperatures of the g-PBST/m-PPZn nanocomposites decreased compared to those of the neat g-PBST copolymers. This phenomenon is attributed to the presence of PPZn in the g-PBST matrix, which can induce more nucleation to form more tiny and imperfect crystals, decreasing the thermal stability. Similar occurrences are reported for related systems, for instance PLA/PPZn, P(3HB-co-3HHX)/PPZn, PBA/PPZn and iPP/PPZn nanocomposites [16,17,25,26].

Fig. 13 reveals the change of storage modulus *E'* versus temperature of g-PBST-30/m-PPZn nanocomposites in a temperature range between −70 °C and 100 °C. These results indicated that the *E'* of g-PBST-30 at −70 °C was around 1340 MPa and decreases as the temperature increases. This finding recommends that the molecular motion of g-PBST in the glassy state was insufficient. When the temperature is higher than

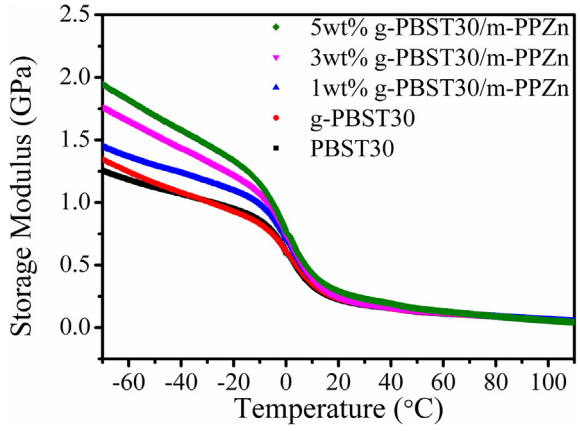

Fig. 13. Dependence of the storage modulus on temperature of PBST-30, g-PBST-30 and g-PBST-30/m-PPZn nanocomposites.

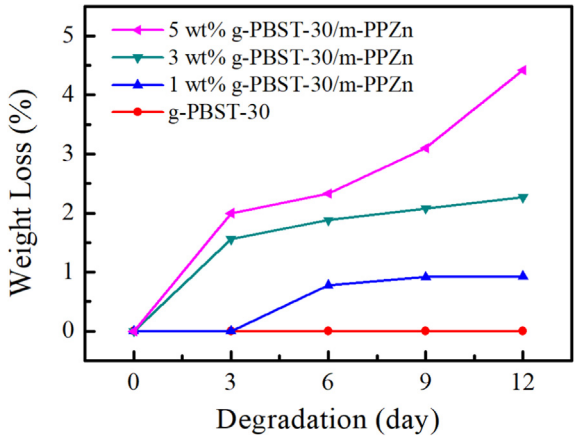

Fig. 14. Dependence of the weight loss on the degradation time for the g-PBST-30/m-PPZn nanocomposites.

glass transition temperature, thermal energy turns out to be analogous to the potential energy barriers of molecular motions. The *E'* of the g-PBST-30/m-PPZn nanocomposites at −70 °C was increased by increasing the loading of m-PPZn. The *E'* values of the corresponding nanocomposites were about 1450, 1760, and 1950 MPa for 1, 3, and 5 wt% loading of m-PPZn into g-PBST-30 polymer matrix, respectively. The enhancement of *E'* may be attributed to the reinforcement effect of the addition of inorganic and stiff m-PPZn and its covalent linkages with g-PBST, improving the rigidity of the g-PBST polymer matrix. Similar results were also obtained for the g-PBST-50/m-PPZn and g-PBST-70/m-PPZn nanocomposites. Detailed *E'* values for all nanocomposites is also illustrated in Table 2.

The effects of m-PPZn on the biodegradation of the g-PBST/m-PPZn nanocomposites were investigated by estimating the weight loss of the specimens during various degradation periods with lipase from *Pseudomonas sp*. Because m-PPZn cannot be degraded by lipase, the change of weight loss after biodegradation is associated merely with the g-PBST copolyesters. Fig. 14 shows the weight losses of g-PBST-30/m-PPZn nanocomposites. The weight loss of neat g-PBST-30 after 12 days degradation was almost zero; the weight losses for the g-PBST-30/m-PPZn nanocomposites were approximately estimated to be 0.93%, 2.27%, and 4.42% with the loading of 1, 3, and 5 wt% m-PPZn, respectively. The weight loss tendencies of g-PBST-50/m-PPZn and g-PBST-70/m-PPZn nanocomposites are similar to those of the g-PBST-30/m-PPZn nanocomposites. Detailed weight loss after 12 days degradation for all nanocomposites is also illustrated in Table 2. The crystalline structures of g-PBST-30 and g-PBST-50 were dominated by the crystalline PBT. The weight loss of g-PBST-50 is slightly higher than those of g-PBST-30, which is attributed to the lower crystallinity of g-PBST-50. The crystalline structure of g-PBST-70 was dominated by the crystalline PBS. Therefore, the degradation rate of g-PBST copolymers varied in the order g-PBSA-70 > g-PBSA-50 > g-PBSA-30. The weight loss increased by increasing the loading of m-PPZn, recommending that the existence of m-PPZn improved the degradation rate of the g-PBST copolymers.

4. Conclusions

New biocompatible and biodegradable g-PBST/m-PPZn nanocomposites were manufactured using the transesterification and polycondensation. FTIR and ^{13}C NMR spectra demonstrate the successful grafting of AA to PBST. Experimental results of WAXD and TEM indicated that the intercalated conformation was formed for the g-PBST/m-PPZn nanocomposites. The addition of m-PPZn in g-PBST matrix enhanced the storage modulus as compared with that of neat g-PBST. The reduction in thermal stability was observed in all g-PBST/m-PPZn systems, which is probably due to the more nucleation to form more tiny and imperfect crystals. The degradation rates of the neat g-PBST copolymers increased in the order of g-PBST-70 > g-PBST-50 > g-PBST-30. The faster degradation rate of g-PBST-70 is a result of the higher content of succinic acid unit and the chain flexibility of polymer backbone. Furthermore, the weight loss increased by increasing the loading of m-PPZn, recommending that the existence of m-PPZn improved the degradation of the g-PBST copolymers.

Acknowledgements

The financial support of this work is provided by the Ministry of Science and Technology (MOST) under Grand MOST 104-2212-E-005-089-MY2 and the Ministry of Education under the project of Innovation and Development Center of Sustainable Agriculture (IDCSA).

Data Availability

If you are sharing data, please ensure you replace the sentences in square brackets with the appropriate links.

References

[1] V. Tserki, P. Matzinos, E. Pavlidou, D. Vachliotis, C. Panayiotou, Biodegradable aliphatic polyesters. Part I. properties and biodegradation of poly(butylene succinate-co-butylene adipate), Polym. Degrad. Stab. 91 (2006) 367–376.
[2] R.J. Muller, I. Kleeberg, W.D. Deckwer, Biodegradation of polyesters containing aromatic constituents, J. Biotech. 86 (2001) 87–95.
[3] M. Nagata, H. Goto, W. Sakai, N. Tsutsumi, Synthesis and enzymatic degradation of poly(tetramethylene succinate) copolymers with terephthalic acid, Polymer 41 (2000) 4373–4376.
[4] S. Luo, F. Li, J. Yu, A. Cao, Synthesis of poly(butylene succinate-co-butylene terephthalate) (PBST) copolyesters with high molecular weights via direct esterification and polycondensation, J. Appl. Polym. Sci. 115 (2010) 2203–2211.
[5] Z. Wei, Lamellae evolution of poly(butylene succinate-co-terephthalate) copolymer induced by uniaxial stretching and subsequent heating, RSC Adv. 4 (2014) 64625–64633.
[6] F. Li, X. Xu, Q. Hao, Q. Li, J. Yu, A. Cao, Effects of comonomer sequential structure on thermal and crystallization behaviors of biodegradable poly(butylene succinate-co-butylene terephthalate)s, J. Polym. Sci. Polym. Phys. 44 (2006) 1635–1644.
[7] M.S. Nikolic, J. Djonlagic, Synthesis and characterization of biodegradable poly (butylene succinate-co-butylene adipate)s, Polym. Degrad. Stab. 74 (2001) 263–270.
[8] V. Ojijo, H. Cele, S. Sinha Ray, Morphology and properties of polymer composites based on biodegradable polylactide/poly[(butylene succinate)-co-adipate] blend and nanoclay, Macromol. Mater. Eng. 296 (2011) 865–877.
[9] N. Jacquel, R. Saint-Loup, J.-P. Pascault, A. Rousseau, F. Fenouillot, Bio-based alternatives in the synthesis of aliphatic-aromatic polyesters dedicated to biodegradable film applications, Polymer 59 (2015) 234–242.
[10] Z. Wei, J. Lin, X. Wang, L. Huang, J. Yu, F. Li, In situ polymerization of biodegradable poly(butylene-co-succinate terephthlate) nanocomposites and their real-time tracking of microstructure, Comp. Sc.i Tech. 117 (2015) 121–129.
[11] Z. Wei, Y. Liu, X. Wang, J. Yu, F. Li, Real-time tracking of the hierarchical structure of biodegradable poly(butylene succinate-co-terephthalate) nanocomposites with fibrous attapulgite nanoparticles, Comp. Sci. Tech. 134 (2016) 201–208.
[12] Z. Wei, Z. Pan, F. Li, J. Yu, Poly(butylene succinate-co-terephthalate) nanofibrous membrane composited with cyclodextrin polymer for superhydrophilic property, RSC Adv. 8 (2018) 1378–1384.
[13] C.S. Wu, Antibacterial and static dissipating composites of poly(butylene adipate-co-terephthalate) and multi-walled carbon nanotubes, Carbon 47 (2009) 3091–3098.
[14] H. Zeng, C. Gao, D. Yan, Poly(ε-caprolactone)-functionalized carbon nanotubes and their biodegradable properties, Adv. Funct. Mater. 16 (2006) 812–818.
[15] P. Pan, Z. Liang, A. Cao, Y. Inoue, Layered metal phosphonate reinforced poly(l-lactide) composites with a highly enhanced crystallization rate, ACS Appl. Mat. Interf. 1 (2009) 402–411.
[16] T. Xu, Y. Wang, D. He, Y. Xu, Q. Li, C. Shen, Nucleation effect of layered metal phosphonate on crystallization of isotactic polypropylene, Polym. Test 34 (2014) 131–139.
[17] F. Yu, P. Pan, N. Nakamura, Y. Inoue, Nucleation effect of layered metal phosphonate on crystallization of bacterial poly[(3-hydroxybutyrate)-co-(3-hydroxyhexanoate)], Macromol. Mater. Eng. 296 (2011) 103–112.
[18] D.M. Poojary, A. Clearfield, Coordinative intercalation of alkylamines into layered zinc phenylphosphonate. crystal structures from X-ray powder diffraction data, J. Am. Chem. Soc. 117 (1995) 11278–11284.
[19] Y. Zhang, K.J. Scott, A. Clearfield, Intercalation of alkylamines into dehydrated and hydrated phenylphosphonates, J. Mater. Chem. 5 (1995) 315–318.
[20] S.K. Murase, M. Aymat, A. Calvet, L.J. del Valle, J. Puiggali, Electrosprayed poly (butylene succinate) microspheres loaded with indole derivatives: a system with

anticancer activity, Euro. Polym. J. 71 (2015) 196–209.
[21] C.S. Wu, Process, characterization and biodegradability of aliphatic aromatic polyester/sisal fiber composites, J. Polym. Environ. 19 (2011) 706–713.
[22] S.K. Rath, M. Patri, S.K. Sharma, K. Sudarshan, P.K. Pujari, Free volume and microstructural investigation of poly(ethylene terephthalate)-g-acrylic acid (PET-g-AA) copolymer films, Rad. Phys. Chem. 79 (2010) 745–750.
[23] J. Zhang, X. Wang, F. Li, J. Yu, Mechanical properties and crystal structure transition of biodegradable poly(butylene succinate-co-terephthalate) (PBST) fibers, Fibers Polym. 13 (2012) 1233–1238.
[24] C.S. Wu, Aliphatic aromatic polyester-polyaniline composites: preparation, characterization, antibacterial activity and conductivities, Polym. Int. 61 (2012) 1556–1563.
[25] N. Wu, H. Wang, Effect of zinc phenylphosphonate on the crystallization behavior of poly(L-lactide), J. Appl. Polym. Sci. 130 (2013) 2744–2752.
[26] Y. Chen, S. Wang, Q. Chen, Z. Xi, C. Wang, X. Chen, X. Feng, R. Liang, J. Yang, Modulated crystallization behavior, polymorphic crystalline structure and enzymatic degradation of poly(butylene adipate): Effects of layered metal phosphonate, Euro. Polym. J. 72 (2015) 222–237.